Journal of Controlled Release 384 (2025) 113934

Contents lists available at ScienceDirect

Journal of Controlled Release

journal homepage: www.elsevier.com/locate/jconrel

Antibody-mediated ratiometric delivery of FLT3 and CDK4/6 dual inhibitors for targeted treatment of acute myeloid leukemia

Zhenzhen Zhai [a], Chenming Li [a], Lin Chen [a], Yan Zhao [a], Xueling Tang [a], Li Cao [b], Huanli Sun [a,*], Zhiyuan Zhong [a,b,*]

[a] State Key Laboratory of Bioinspired Interfacial Materials Science, Biomedical Polymers Laboratory, College of Chemistry, Chemical Engineering and Materials Science, Soochow University, Suzhou 215123, PR China
[b] College of Pharmaceutical Sciences, Soochow University, Suzhou 215123, PR China

ARTICLE INFO

Keywords:
Molecular targeted drug
Blood cancer
Combination therapy
Targeted delivery
Nanomedicines

ABSTRACT

Molecularly targeted agents have revolutionized the paradigm of cancer treatment; however, their efficacy is often downplayed by rapid clearance in vivo, inferior cellular delivery and drug resistance. The combination of targeted drugs could improve the clinical efficacy only to some extent, due to overlapping toxicities and difficulty in maintaining certain drug ratios. Here, we report on ratiometric codelivery of FLT3 and CDK4/6 dual inhibitors, gilteritinib and palbociclib, by daratumumab-decorated polymersomes (GIPA@DP) for high-efficacy targeted therapy of acute myeloid leukemia (AML). GIPA@DP showed synergistic anti-AML effects on MV-4-11 cells, with a half-maximal inhibitory concentration of ca. 2.6 ng/mL for each drug, which was further reduced to below 1 ng/mL by pretreating the cells with all-trans retinoic acid. GIPA@DP maintained an essentially constant GI/PA ratio in vivo and actively targeted AML cells at different leukemia sites. Selective AML-targeting in conjunction with ratiometric drug codelivery and synergistic anti-AML effects of GIPA@DP collectively led to significant survival benefits in CD38-upregulated MV-4-11 and Molm-13-Luc AML models, outperforming the nontargeted control (GIPA@P) and a mixture of two targeted single drug formulations (GI@DP + PA@DP). This targeted ratiometric delivery of dual inhibitors provides a new treatment strategy for AML and other malignancies.

1. Introduction

The emergence of molecular targeted drugs that are specific to tumor biomarkers has revolutionized the treatment of a variety of malignancies, including acute myeloid leukemia (AML) [1–4]. AML is among the most intractable blood cancers and is mortal to the majority of patients, with a 5-year overall survival rate of less than 30 % [5–7]. Recent approval of small-molecule targeted drugs specific for mutated or overexpressed proteins, such as gilteritinib (GI) and midostaurin inhibitors against mutated FLT3, has advanced the treatment of AML [8–11]. Nevertheless, the success and efficacy of small-molecule targeted drugs, including FLT3 inhibitors, are typically hindered by rapid in vivo metabolism, low cellular delivery and drug resistance, leading to inferior clinical outcomes as monotherapies [12,13].

The rational combination of FLT3 inhibitors with drugs targeting other signaling pathways can circumvent drug resistance and enhance therapeutic efficacy via potential synergy [14–16]. Cyclin-dependent kinase 4 and 6 (CDK4/6) inhibitors that target overactivated CDK4/6 in various cancers, including AML, have been shown to overcome resistance to certain drugs [17–20]. Palbociclib (PA), a clinically approved CDK4/6 inhibitor, was reported to regulate FLT3 transcription and overcome resistance to FLT3 inhibitors, thus generating synergistic effects [16,21]. However, the combination efficacy of small-molecule drugs remains hampered by several challenges, such as uncontrollable in vivo drug ratios as a result of inherent differences in physicochemical properties and overlapping toxicities resulting from high-dose administration [22].

Nanomedicines provide a promising approach to increase drug efficacy via ratiometric drug codelivery and diminish toxicity via a reduction in drug dosage [23–25]. In a typical example, the commercially available CPX-351 liposome injection maintains a synergistic ratio of cytarabine to daunorubicin in vivo, thus exhibiting superior efficacy in

* Corresponding authors at: State Key Laboratory of Bioinspired Interfacial Materials Science, Biomedical Polymers Laboratory, College of Chemistry, Chemical Engineering and Materials Science, Soochow University, Suzhou 215123, PR China.
E-mail addresses: sunhuanli@suda.edu.cn (H. Sun), zyzhong@suda.edu.cn (Z. Zhong).

https://doi.org/10.1016/j.jconrel.2025.113934
Received 15 April 2025; Received in revised form 20 May 2025; Accepted 4 June 2025
Available online 6 June 2025
0168-3659/© 2025 Elsevier B.V. All rights are reserved, including those for text and data mining, AI training, and similar technologies.

AML patients compared with standard 7 + 3 chemotherapy (i.e., the free drug combination) [26–28]. Nevertheless, CPX-351, which is based on cytotoxic chemotherapeutics, is still associated with severe adverse effects, and its therapeutic efficacy remains suboptimal because of ineffective drug delivery. Actively targeted nanomedicines, particularly our strategy that employs all-trans retinoic acid (ATRA)-mediated exogenous CD38 upregulation to enhance AML targeting by daratumumab-engineered nanomedicines [29–32], are anticipated to significantly amplify the synergistic effects of drug combinations.

In this study, we report on ratiometric codelivery of GI and PA dual inhibitors by daratumumab-decorated polymersomes (GIPA@DP) for coinhibition of FLT3 and CDK4/6, thus potentiating targeted therapy of AML (Scheme 1). The coinhibition of FLT3 and CDK4/6 can not only synergistically induce cell apoptosis but also promote the differentiation of AML cells to nonmalignant cells. Daratumumab is an FDA-approved antibody that specifically targets CD38 and has preliminarily demonstrated potential in the treatment of AML patients [33,34]. Strikingly, GIPA@DP selectively targeted CD38-upregulated AML cells, exhibited enhanced synergistic effects, and maintained a stable drug ratio during circulation and accumulation at different leukemic sites, leading to potent leukemia inhibition and a significant survival benefit in two different AML models. In particular, 50 % of the mice bearing CD38-upregulated MV-4-11 AML achieved complete remission following treatment with GIPA@DP, significantly outperforming all the control groups. Compared with liposomal CPX-351, GIPA@DP has high stability, controlled drug release and specific CD38 targeting, which not only enables selective targeting to AML cells but also ensures a more stable drug ratio in vivo. Furthermore, GIPA@DP elicits anti-AML effects via targeted delivery of molecular targeted drugs, offering a more precise and safer therapeutic approach than chemotherapeutics-based CPX-351.

2. Experimental section

2.1. Cells and AML models

Molm-13-Luc AML cells and normal human T cells were kindly provided by Dr. Fengtao You from Persongen Bio Therapeutics (Suzhou) Co., Ltd. Mouse peripheral blood mononuclear cells (PBMCs) were isolated from the peripheral blood of healthy BALB/c mice. MV-4-11 human AML cells were purchased from the National Collection of Authenticated Cell Cultures. The cells were cultured in a humidified atmosphere of 5 % CO_2 at 37 °C in RPMI 1640 medium (Gibco) supplemented with 10 % fetal bovine serum (FBS) and 1 % penicillin/streptomycin (Genom Biopharmaceutical Technology Co., Ltd., China). CD38-upregulated AML cells were obtained via pretreatment with ATRA (1 μM) for 48 h. Patient-derived primary AML cells isolated from the bone marrow aspirates of an AML patient and human PBMCs isolated from a healthy donor were kindly provided by Prof. Yang Xu and Dr. Tianhui Liu from the First Affiliated Hospital of Soochow University.

All the animal experiments were approved by the Animal Care and Use Committee of Soochow University (Suzhou, China), and all the protocols of the animal studies conformed to the Guide for the Care and Use of Laboratory Animals (Approval Nos: SYXK 2021–0065, 202404A0287, 202409A0221, and 202409A0226). Orthotopic MV-4-11

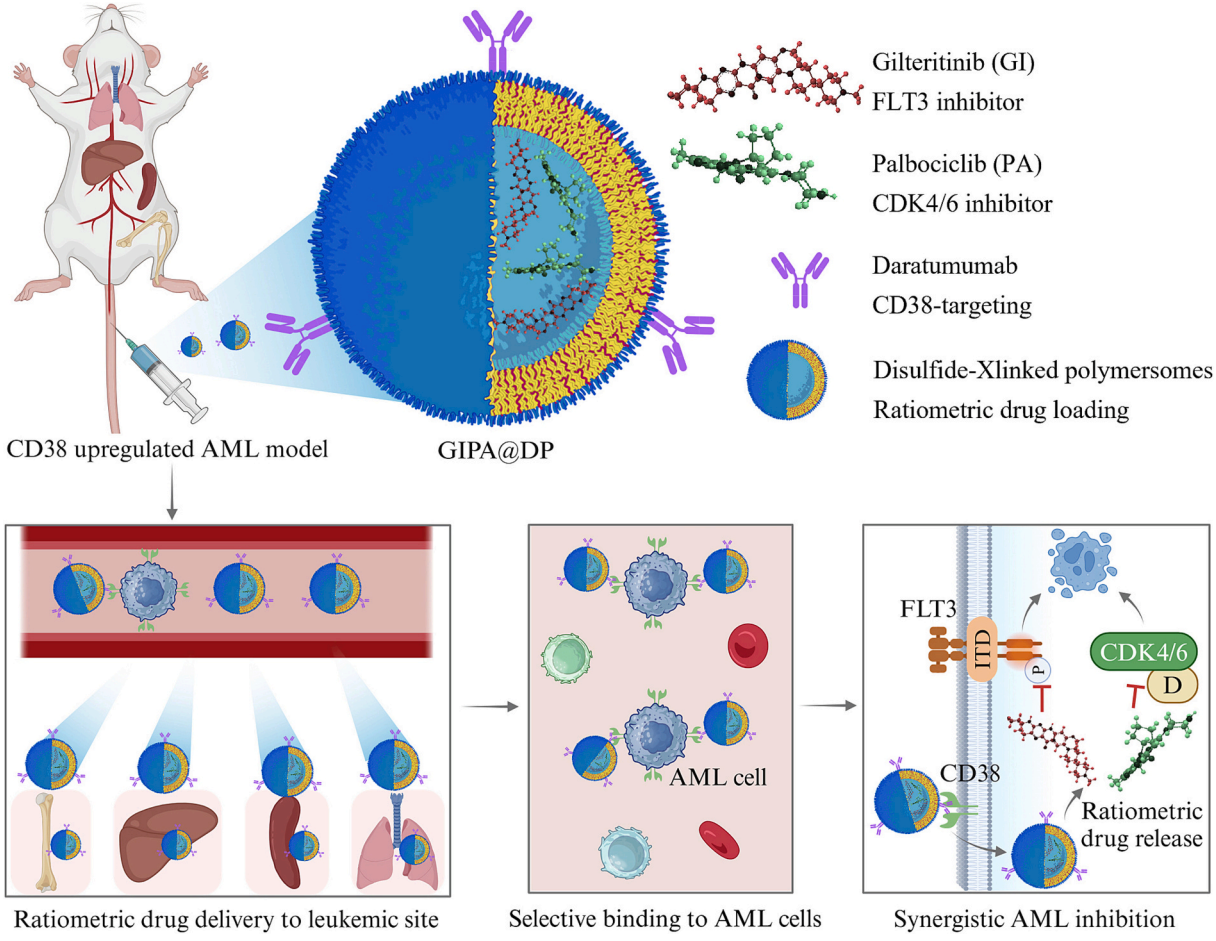

Scheme 1. Schematic showing the composition of GIPA@DP, which, after intravenous injection, ratiometrically delivered FLT3 and CDK4/6 inhibitors to the leukemic site, selectively targeted AML cells and ratiometrically released drugs inside cells, thus leading to potent targeted therapy in a CD38-upregulated AML model.

and Molm-13-Luc AML models were established by injecting 5×10^5 MV-4-11 or Molm-13-Luc cells into the tail vein of each B-NDG mouse (Biocytogen, 6–8 weeks old). CD38-upregulated models were established by intraperitoneal injection of ATRA (200 μL, 10 mg/kg) for two consecutive days prior to each injection with daratumumab-polymersome formulations.

2.2. Materials and characterizations

Gilteritinib (GI, 99.8 %) and palbociclib (PA, 99.8 %) were purchased from Med Chem Express. The APC-Cy7 Zombie NIR™ fixable viability kit (Cat: 423106), APC-anti-mouse/human CD11b antibody (Cat: 101211), PE anti-human CD33 (Cat: 366607), PE anti-human CD45 antibody (Cat: 304008), APC anti-human CD45 antibody (Cat: 304012), and FITC anti-human CD45 antibody (Cat: 304006) were purchased from BioLegend. The additional materials and characterizations used in this work are detailed in the Supporting Information.

2.3. Preparation of GIPA@P

GI and PA were coloaded into chimaeric polymersomes based on the poly(ethylene gly*col*)-*b*-poly(trimethylene carbonate-*co*-dithiolane trimethylene carbonate)-*b*-N-terminal acetylated poly(aspartic acid) (PEG-P(TMC-DTC)-Ac-KD_{10}) copolymer through electrostatic interactions at mass feeding ratios of 2:1, 1:1 and 1:2. The detailed synthesis procedure of the copolymer is provided in the Supporting Information. Taking the 1:1 ratio as an example, 0.8 mL of the GI solution in dimethyl sulfoxide (DMSO, 5 mg/mL), 0.4 mL of the PA solution (DMSO, 10 mg/mL) and 1 mL of the polymer solution in DMSO (40 mg/mL) were mixed uniformly and then slowly injected into 17.8 mL of the 4-(2-hydroxyethyl)-1-piperazine ethanesulfonic acid (HEPES) buffer (5 mM, pH 6.8) at 37 °C and 300 rpm. After overnight incubation at 37 °C, the suspension was dialyzed (MWCO: 3.5 kDa) against HEPES buffer (5 mM, pH 7.4) to obtain $GIPA_{1/1}$@P. Subsequently, it was concentrated to a polymersome concentration of 20 mg/mL in an ultrafiltration tube (Vivaspin, MWCO: 10 kDa). Single drug polymersomes, namely GI@P and PA@P, were prepared similarly. The size and size distribution of GIPA@P, GI@P and PA@P were determined by dynamic light scattering (DLS). The amounts of GI and PA in the polymersomes were determined via high performance liquid chromatography (HPLC). The drug loading content (DLC) and drug loading efficiency (DLE) were calculated via the following formulas:

$$\text{DLC (wt.\%)} = \frac{\text{weight of loaded GI or PA}}{\text{total weight of drug loaded polymersomes}} \times 100$$

$$\text{DLE (\%)} = \frac{\text{weight of loaded GI or PA}}{\text{weight of GI or PA in feed}} \times 100$$

The storage stability of $GIPA_{1/1}$@P at 4 °C was assessed by monitoring the size change and drug leakage. The drug release profiles of $GIPA_{1/1}$@P were studied in triplicate in HEPES (5 mM, pH 7.4) or HEPES containing 10 mM glutathione (GSH). Briefly, 0.5 mL of $GIPA_{1/1}$@P (P: 2 mg/mL) was dialyzed (MWCO: 14 kDa) against 20 mL of release medium at 37 °C and 100 rpm. Five milliliters of release medium was collected at 1, 2, 4, 6, 8, 10, 12 and 24 h for quantification of the released drugs by HPLC, and fresh dialysate was replenished after each sampling.

Blank polymersomes dispersed in D_2O were prepared by injecting a polymer solution in DMSO-d_6 into D_2O with subsequent ultracentrifugation and redispersion in D_2O, and then characterized by ^{1}H NMR spectroscopy. The experimental details on the in vitro and in vivo anti-AML activity of GIPA@P, as well as GIPA@P induced cell cycle arrest, cell apoptosis, mRNA regulation and cell differentiation, are described in the Supporting Information.

2.4. Preparation of GIPA@DP

GIPA@DP was fabricated by clicking daratumumab (Dar) onto the surface of azide-functionalized GIPA@P, which was obtained via the addition of 2 wt% N_3-PEG-P(TMC-DTC) (7.9-(15.0-2.0) kg/mol) during assembly. To enable the click reaction, Dar was first reacted with NHS-PEG_4-DBCO at a molar ratio of 1:3. In brief, 0.1 mL of Dar solution (20 mg/mL) was mixed with 0.1 mL of PBS (PB: 10 mM, NaCl: 150 mM, pH 8.5), and 2.6 μL of NHS-PEG_4-DBCO solution in DMSO (10 mg/mL) was added for an overnight reaction at 25 °C and 100 rpm. Dar-DBCO was then obtained via ultrafiltration (Vivaspin, MWCO: 10 kDa) twice using PBS (PB: 10 mM, NaCl: 150 mM, pH 7.4). The DBCO functionality of Dar-DBCO was characterized by MALDI-TOF-MS with a Dar concentration of 1 mg/mL. Subsequently, azide-functionalized GIPA@P was reacted with Dar-DBCO at different Dar-to-azide molar ratios of 0.25:1, 0.5:1, and 1:1 to obtain GIPA@DP with different Dar densities. Taking the 0.5:1 ratio as an example, 22.7 μL of Dar-DBCO solution (5.3 mg/mL) was added to 100 μL of azide-functionalized GIPA@P (20 mg/mL), followed by an overnight reaction at 25 °C and 100 rpm. The mixture was then diluted with HEPES (5 mM, pH 7.4) and subjected to ultracentrifugation (58 krpm, 1 h) to remove unreacted Dar-DBCO, yielding GIPA@DP. The amount of Dar conjugated to GIPA@DP was calculated on the basis of the quantification of unreacted Dar-DBCO in the supernatant via HPLC.

2.5. In vitro selective AML binding of GIPA@DP

To enable effective CD38 targeting, $CD38^{low}$ Molm-13-Luc and MV-4-11 AML cells were pretreated with 1 μM ATRA for 48 h to increase CD38 expression, referred to as CD38-upregulated cells, prior to incubation with GIPA@DP. The in vitro AML selectivity of GIPA@DP in a coculture system of CD38-upregulated AML cells and normal human T cells was studied via flow cytometry using Cy5-labeled polymersomes (P-Cy5 and DP-Cy5). A total of 1×10^6 CD38-upregulated MV-4-11 or Molm-13-Luc cells were stained with 1 μL of Dil solution (1 mg/mL) in the incubator for 15 min and then at 4 °C for 10 min, followed by thorough washing. First, 0.9 mL of Dil-stained AML cells (5×10^5 cells/well) along with 0.9 mL of T cells (5×10^5 cells/well) were added to a 6-well plate. Then, 0.2 mL of P-Cy5 or DP-Cy5 (P: 5 μg/mL, Cy5: 57.5 nM) was added. After incubation for 4 h, the cells were washed, collected and analyzed via flow cytometry.

The selectivity of DP-Cy5 to patient-derived primary AML cells was investigated similarly. Primary AML cells were pretreated with 1 μM ATRA for 48 h and stained with carboxyfluorescein succinimidyl ester (CFSE). A mixture of 2×10^5 primary AML cells and 2×10^5 human PBMCs was seeded into a 12-well plate, followed by incubation with P-Cy5 or DP-Cy5 (P: 5 μg/mL, Cy5: 57.5 nM) for 4 h. The cells were then harvested and sequentially stained with an APC-Cy7 Zombie NIR™ fixable viability kit and PE anti-human CD33 antibody prior to flow cytometry analysis.

The selective AML binding of DP-Cy5 was further visualized via confocal laser scanning microscopy (CLSM). CD38-upregulated MV-4-11 and Molm-13-luc cells were stained with Dil as described above. T cells (5×10^6) were stained with 1 μL of 1 μM CFSE staining solution for 5 min. A total of 0.45 mL of AML cells (5×10^5 cells/well) and 0.45 mL of T cells (5×10^5 cells/well) were plated onto a poly-L-lysine-pretreated coverslip in a 6-well plate. Then, 100 μL of P-Cy5 or DP-Cy5 (P: 300 μg/mL, Cy5: 3.5 μM) was added, and the mixture was incubated for 4 h at 37 °C. Afterwards, the cells were washed with PBS, fixed with 1 mL of 4 % paraformaldehyde (PFA) for 15 min, stained with DAPI and washed with PBS. The cells on the coverslip were then transferred to a microscope slide and imaged via CLSM.

2.6. In vitro anti-AML activity of GIPA@DP

CD38-upregulated Molm-13-Luc and MV-4-11 AML cells were plated

in 96-well plates (80 μL, 2 × 10^4 cells/well) and then incubated with GIPA@DP at different Dar densities, GIPA@P or free GIPA, for 48 h (n = 6). Subsequently, 10 μL of CCK-8 solution was added, and the mixture was handled similarly to above to calculate the cell viability. The synergistic anti-AML effects of GIPA@DP with different GI-to-PA ratios were similarly evaluated in CD38-upregulated MV-4-11 cells, with GI@DP and PA@DP used as controls. The cytotoxicity of GIPA@DP plus ATRA to normal cells, including mouse PBMCs, DC 2.4 cells and human T cells, was assessed similarly at GI or PA concentrations of 0.01–10 μg/mL (n = 6).

GIPA@DP-mediated apoptosis was then studied in CD38-upregulated AML cells via an Annexin V-APC/7-AAD staining apoptosis kit. The procedure was the same as those used in the cell apoptosis study with GIPA@P, which served as a control. The concentrations of GI and PA were each set at 5 ng/mL. GIPA@DP-mediated apoptosis in patient-derived primary AML cells and human PBMCs was studied similarly, with a GI or PA concentration of 2 μg/mL. The primary AML cells were stained with PE anti-human CD33 antibody along with Annexin V-APC/7-AAD. The percentage of apoptosis in primary AML cells and human PBMCs was determined by subtracting the apoptosis rate of control cells treated with PBS.

2.7. RNA-seq analysis

The underlying mechanism of the combination effect of GIPA@DP was investigated via RNA sequencing (RNA-seq). Fifteen milliliters of MV-4-11 cells (3 × 10^6 cells) in culture flasks were incubated with PBS, $GIPA_{1/1}$@P, or $GIPA_{1/1}$@DP (CD38-upregulated cells) for 48 h at GI and PA concentrations of 0.5 ng/mL. After incubation, the cells were collected, and 1.5 mL of Trizol was added with gentle pipetting. The samples were then stored at -80 °C. Subsequent testing and RNA-seq library construction were performed at Beijing Novogene Bioinformatics Technology Co., Ltd.

2.8. Pharmacokinetic study of GIPA@P and GIPA@DP

Two hundred microliters of free GIPA, $GIPA_{1/1}$@P or $GIPA_{1/1}$@DP was injected into the tail vein of 9-week-old female BALB/c mice (n = 3). Blood was collected from the mouse orbital sinus at 10 min, 20 min, 40 min, 1 h, 2 h, 4 h, 8 h, 12 h, 24 h, and 48 h and centrifuged at 3000 rpm for 10 min. Thirty microlitres of plasma was mixed with 1 mL of methanol containing 20 mM dithiothreitol (DTT) and incubated overnight in a shaker to extract the GI and PA contents. After centrifugation at 3000 rpm for 10 min, the supernatant was collected, and the methanol was evaporated. Subsequently, 0.1 mL of methanol was added to redissolve the residue, and the drug concentration was determined via HPLC. The GI-to-PA mass ratio in the blood was then calculated. PKsolver was used to fit the elimination phase half-life ($t_{1/2,\beta}$).

2.9. In vivo biodistribution and AML selectivity of GIPA@DP

The biodistribution of GIPA@DP was studied in an orthotopic MV-4-11 AML model. To enable imaging, Did was coloaded into the polymersomes, resulting in $GIPA_{1/1}$/Did@P and $GIPA_{1/1}$/Did@DP. The mice were randomly divided into two groups when obvious symptoms of illness were observed on day 16 (n = 4). For the $GIPA_{1/1}$/Did@DP group, 200 μL of $GIPA_{1/1}$/Did@DP (GI: 16 mg/kg, Did: 0.2 μg per mouse) was intravenously injected into a CD38-upregulated model on day 18. Mice intravenously injected with $GIPA_{1/1}$/Did@P on day 18 were used as controls. At 1 h, 2 h, 4 h and 8 h post-injection of the polymersomes, the mice were imaged via a near-infrared fluorescence imaging system. After 8 h of imaging, the mice were sacrificed, and their major organs and leg bones were collected for ex vivo imaging. The data were analyzed via Living Image 2.6 software. The organs and leg bones were subsequently weighed, soaked in 0.95 mL of methanol each and homogenized. Afterward, 50 μL of methanol solution containing 400 mM DTT was added, and the samples were shaken at 37 °C and 200 rpm for 12 h to release the GI and PA. After centrifugation at 6000 rpm for 10 min, the supernatant was collected, and the solvent was evaporated. Finally, 0.1 mL of methanol was added to redissolve the sample, which was then filtered through a 0.22 μM filter and analyzed via HPLC.

The in vivo AML selectivity of GIPA@DP in orthotopic MV-4-11 AML-bearing mice was studied using Cy5-labeled polymersomes (DP-Cy5), with P-Cy5 serving as a control. Mice with obvious symptoms of illness were randomly divided into two groups and intravenously injected with P-Cy5 or DP-Cy5 (P: 0.8 mg per mouse, Cy5: 0.2 μg per mouse) (n = 3). DP-Cy5 was injected into the tail vein of a CD38-upregulated model established as described above. At 4 h post-injection, blood was collected from the orbital sinus. Then, the mice were sacrificed, and the livers, spleens, lungs, and leg bones were isolated. Half of the spleen and leg bones were fixed with 4 % PFA solution, embedded in paraffin, sectioned, and stained with DAPI and FITC anti-human-CD45 for CLSM imaging. The residual tissues were homogenized, subjected to red blood cell lysis, stained with PE anti-human CD45 antibody and fixed with 0.5 % PFA for flow cytometry analysis.

2.10. In vivo anti-AML activity of GIPA@DP

The anti-AML activity of GIPA@DP at a GI/PA ratio of 1/1 was subsequently studied in an orthotopic MV-4-11 mouse model. The mice were randomly divided to receive different treatments, including PBS, GI@P, PA@P, free GIPA, GIPA@P, GI@DP+PA@DP, and GIPA@DP (n = 9). For the GI@DP+PA@DP and GIPA@DP groups, a CD38-upregulated model that received daily intraperitoneal injections of ATRA from day 1 to day 12 was used. Treatments with different GI/PA formulations were initiated on day 3 post-modeling via tail vein injection every 2 days for a total of 6 treatments. The GI and PA dosages were both set at 8 mg/kg. The body weights of the mice were recorded every 3 days, and survival was continuously monitored. On day 45, 4 mice from each of the GIPA@P and GIPA@DP groups were sacrificed, and the major organs, peripheral blood and hindlimbs were collected. The mice in the PBS group were sacrificed at their endpoint (day 18) for comparison. Portions of the liver, spleen, lung and hindlimbs were homogenized and stained with an APC anti-human CD45 antibody to determine leukemia infiltration via flow cytometry. The residual major organs and hindlimbs were fixed with 4 % PFA, embedded in paraffin, and subjected to hematoxylin and eosin (H&E) staining and tartrate-resistant acid phosphatase (TRAP) staining for histological and osteoclast analysis. The structure and bone tissue morphology of the femur and tibia were imaged via micro-CT and analyzed via NRecon software.

An orthotopic Molm-13-Luc AML model was further used to confirm the anti-AML activity of GIPA@DP. On day 3 post-inoculation, the mice were randomly divided and treated with PBS, free GIPA, GIPA@P, GI@DP+PA@DP, or GIPA@DP at the same dosage and schedule as those used for the MV-4-11 model (n = 5). A CD38-upregulated model was used for the last two groups. Body weight was recorded every 3 days during the treatment period, and survival was continuously monitored. Leukemia progression was monitored weekly via bioluminescence imaging, in which the mice were intraperitoneally injected with D-luciferin potassium salt (1.5 mg per mouse) 10 min prior to imaging. The images were analyzed via Living Image 2.6 software.

2.11. Statistical analysis

All the data are presented as the means ± standard deviations (means ± SDs). Differences between two groups were analyzed via Student's t-test, and differences among three or more groups were analyzed via one-way analysis of variance (ANOVA) with Tukey's multiple comparisons test. Survival curves were constructed via the Kaplan–Meier method, and differences between groups were compared via the log-rank (Mantel–Cox) test. *$p < 0.05$ indicates a significant difference, and **$p < 0.01$, ***$p < 0.001$ and ****$p < 0.0001$ indicate

highly significant differences.

3. Results and discussion

3.1. Preparation and synergistic anti-AML activity of GIPA@P

To improve the synergistic efficacy of GI and PA, they were coloaded into chimaeric polymersomes with a negatively charged inner surface via electrostatic interactions, yielding polymersomal dual-drug nanoformulations (denoted as GIPA@P). Chimaeric polymersomes were assembled from the PEG-P(TMC-DTC)-Ac-KD_{10} copolymer (**Fig. S1**), which was synthesized according to our previous report with slight modifications [35]. The ^{1}H NMR spectrum of chimaeric polymersomes in D_2O showed strong signals from PEG, whereas the signals associated with hydrophobic P(TMC-DTC) were very weak, and the signals from Ac-KD_{10} were undetectable (**Fig. S2**). These observations suggest that PEG is predominantly located on the outer surface of the polymersomes, while Ac-KD_{10} is located on the inner surface. By adjusting the feeding drug ratios, GIPA@P with different GI-to-PA mass ratios of 2.1:1, 1:1 and 1:1.9 were obtained, which were defined as $GIPA_{2/1}$@P, $GIPA_{1/1}$@P, and $GIPA_{1/2}$@P, respectively (**Table S1**). Compared with PA@P (45 nm), GIPA@P exhibited a smaller size of 27–43 nm, which increased with increasing PA content (**Fig. S3A**). Both GIPA@P and single drug polymersomes (GI@P, PA@P) had narrow size distributions, with polydispersity indices of 0.08–0.11 (**Table S1**). GIPA@P presented a spherical hollow structure and high stability during 60 days of storage at 4 °C with limited drug leakage (< 5 %) (**Fig. S3B—D**). Owing to the presence of disulfide crosslinking, GIPA@P showed slow drug release under physiological conditions, while exposure to 10 mM GSH triggered almost complete release of GI and PA in 24 h with similar release kinetics (Fig. 1A). The superb stability of GIPA@P, characterized by limited drug leakage, combined with the GSH-triggered simultaneous release of GI and PA, is beneficial for ratiometric drug delivery. Anti-AML studies in MV-4-11 and Molm-13-Luc AML cells demonstrated that GIPA@P with three different GI-to-PA ratios had synergistic effects, with a low combination index (CI) of 0.39–0.47 (**Table S2**). $GIPA_{1/1}$@P, with the lowest CI value, potently inhibited MV-4-11 cells, with a half-maximal inhibitory concentration (IC_{50}) of 2.2 ng/mL for both GI and PA, which were 2.8- and 33.1-fold lower than those of GI@P (6.1 ng/mL) and PA@P (72.8 ng/mL), respectively (Fig. 1B). Similarly, GIPA@P presented markedly lower IC_{50} values in Molm-13-Luc cells than did GI@P, PA@P and free GIPA (**Fig. S4**).

FLT3 inhibitors and CDK4/6 inhibitors have been reported to arrest the cell cycle at the G0/G1 phase by inhibiting FLT3 receptor phosphorylation and CDK4/6 activity, respectively, thus inducing cell apoptosis and differentiation [36,37]. We then investigated the

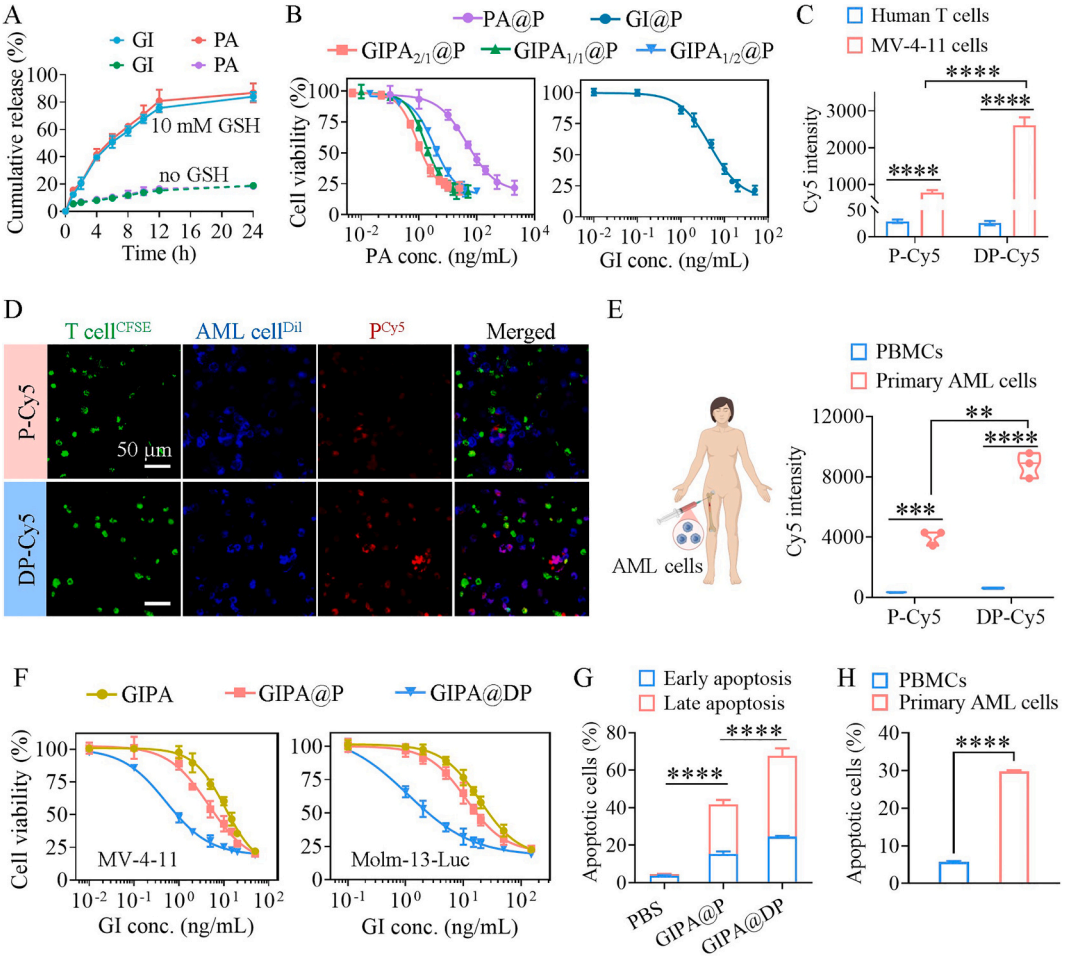

Fig. 1. Characterization and in vitro anti-AML activity of GIPA@DP. (A) In vitro drug release curves of GIPA@P under different conditions (n = 3). (B) Anti-AML activity of GIPA@P at different drug ratios in MV-4-11 cells, with GI@P and PA@P used as controls. (C) Selective binding of DP-Cy5 to CD38-upregulated MV-4-11 cells in a coculture system with T cells (n = 3). P-Cy5 was used as a control. (D) CLSM images showing cocultured CD38-upregulated MV-4-11 cells and T cells after incubation with DP-Cy5 or P-Cy5 (scale bars: 50 μm). (E) Selective binding of DP-Cy5 to CD38-upregulated patient-derived primary AML cells in a coculture system with human PBMCs (n = 3). (F) Viability of CD38-upregulated MV-4-11 and Molm-13-Luc cells after treatment with different formulations for 48 h (n = 6). (G) Apoptosis analysis of CD38-upregulated MV-4-11 cells following 48 h of incubation with PBS, GIPA@P or GIPA@DP (n = 3). (H) Apoptosis analysis of CD38-upregulated patient-derived primary AML cells or human PBMCs following 48 h of incubation with GIPA@DP (n = 3).

synergistic effects of GIPA@P on cell cycle arrest and cell apoptosis. As shown in **Fig. S5A**, GIPA@P with different drug ratios efficiently induced G0/G1 phase arrest in MV-4-11 cells, and $GIPA_{1/1}$@P was most effective, with 66.6 % of the cells in the G0/G1 phase, which was significantly greater than that of GI@P, PA@P and free $GIPA_{1/1}$ (42.1–49.3 %). Similar results were also observed in Molm-13-Luc cells (**Fig. S5B**). Accordingly, compared with single drug polymersomes and free GIPA, $GIPA_{1/1}$@P induced the highest level of cell apoptosis in the two different AML cell lines (**Fig. S6**). For example, treatment with $GIPA_{1/1}$@P induced apoptosis in 49.0 % of MV-4-11 cells, which was significantly greater than that of GI@P (9.9 %), PA@P (8.2 %) and free $GIPA_{1/1}$ (27.6 %). Previous reports have shown that treatment with FLT3 inhibitors such as GI increases the expression of FLT3 in AML cells [38,39], which may limit its therapeutic efficacy. The results of quantitative reverse transcription polymerase chain reaction (qRT–PCR) revealed that treatment with $GIPA_{1/1}$@P effectively reversed the upregulation of FLT3 mRNA induced by GI@P, in which the FLT3 mRNA level was downregulated by 42 % and 30 % compared with that in cells treated with GI@P and PBS, respectively. Moreover, treatment with $GIPA_{1/1}$@P significantly downregulated the expression level of PIM1 mRNA to 16.6 %, which was markedly lower than that of PA@P (87.4 %) and GI@P (36.0 %) (**Fig. S7A**). Elevated PIM1 expression is observed in various malignancies, including AML, and is correlated with poor prognosis [40]. In addition to causing cell apoptosis, FLT3 and CDK4/6 inhibition can also promote the differentiation of AML cells [37,41]. As expected, $GIPA_{1/1}$@P facilitated the differentiation of MV-4-11 cells in a concentration- and time-dependent manner, as evidenced by the increased surface expression of CD11b, which was superior to that of GI@P and PA@P (**Fig. S7B**). In orthotopic MV-4-11 AML-bearing mice, treatment with $GIPA_{1/1}$@P or $GIPA_{1/2}$@P significantly prolonged survival by more than 2.5-fold without causing toxicity, with $GIPA_{1/1}$@P demonstrating greater efficacy (**Fig. S8**). Given the stronger synergistic effects observed with $GIPA_{1/1}$@P both in vitro and in vivo than that with other drug ratios, $GIPA_{1/1}$@P was selected for further studies and designated GIPA@P unless otherwise specified.

3.2. *GIPA@DP selectively targets AML cells and potently inhibits AML in vitro*

GIPA@DP with averages of 1.5, 3 and 6 Dar per polymersome, denoted as GIPA@$D_{1.5}$P, GIPA@D_3P and GIPA@D_6P, respectively, was prepared by clicking DBCO-conjugated Dar (**Fig. S9A**) onto the surface of azide-functionalized GIPA@P. GIPA@DP with different Dar densities or different GI-to-PA ratios displayed a size of 37–39 nm, which was slightly larger than that of nontargeted GIPA@P (34 nm), and a narrow PDI of 0.09–0.12 (**Fig. S9B and Table S3**). Moreover, the DLE of GI and PA in GIPA@DP was 64.3–69.6 %, similar to that of GIPA@P, indicating that no drug leakage occurred during the Dar conjugation process. To enable selective AML targeting by GIPA@DP, CD38-upregulated AML cells pretreated with ATRA were utilized. Our previous work demonstrated that ATRA stimulation can upregulate CD38 levels on $CD38^{low}$AML cells by up to 20-fold, thus enabling CD38-targeted therapy [32]. Compared with nontargeted GIPA@P, GIPA@DP at different Dar densities had significantly greater anti-AML effects on CD38-upregulated MV-4-11 and Molm-13-Luc cells (**Fig. S10**). GIPA@DP with 3 Dar on the surface had the most potent effect and was used for subsequent studies. Moreover, GIPA@DP with different GI-to-PA ratios had strong synergistic effects in CD38-upregulated MV-4-11 cells, with CI values (0.39–0.46) similar to those of nontargeted GIPA@P (**Fig. S11** and **Table S4**). The AML selectivity of GIPA@DP was first investigated via incubation of Cy5-labeled polymersomes with a coculture system of AML cells and T cells. Notably, DP-Cy5 selectively targeted CD38-upregulated MV-4-11 and Molm-13-Luc cells, which presented 26- and 123-fold stronger Cy5 fluorescence intensities than did T cells (Fig. 1C, **S12A**). Moreover, the uptake of DP-Cy5 by the two AML cell lines was also 3-fold greater than that of nontargeted P-Cy5. CLSM images further confirmed the selective binding of DP-Cy5 to CD38-upregulated AML cells and enhanced cellular uptake compared with that of P-Cy5 (Fig. 1D**, S12B**). The selectivity of DP-Cy5 was further confirmed in a coculture system of patient-derived primary AML cells and human PBMCs isolated from a healthy donor, in which primary AML cells displayed 14.5-fold stronger Cy5 fluorescence than did human PBMCs (Fig. 1E).

As a result, GIPA@DP potently inhibited the proliferation of CD38-upregulated MV-4-11 cells, yielding an IC_{50} of 0.9 ng/mL for both GI and PA, which were only 1/15 and 1/7 of the IC_{50} values for GIPA and GIPA@P, respectively. Similarly, the anti-AML activity of GIPA@DP in CD38-upregulated Molm-13-Luc cells was also significantly greater than that of all the other control formulations (Fig. 1F). Importantly, GIPA@DP exhibited no obvious cytotoxicity against normal human T cells, DC 2.4 cells or mouse PBMCs with ATRA stimulation, even at high GI or PA concentrations of 10 μg/mL (**Fig. S13**). Apoptosis analysis of CD38-upregulated MV-4-11 cells revealed that treatment with GIPA@DP dramatically increased the cell apoptosis rate from 4.5 % (PBS) to 67.7 %, which was greater than that of GIPA@P (41.7 %) (Fig. 1G**, S14**). Moreover, GIPA@DP induced apoptosis in 29.9 % of the primary AML cells, in contrast to only 5.7 % apoptosis in human PBMCs from a healthy donor (Fig. 1H). Additionally, GIPA@DP treatment significantly promoted the differentiation of CD38-upregulated MV-4-11 and Molm-13-Luc cells (**Fig. S15**).

3.3. *RNA-seq analysis reveals the signaling pathways modulated by GIPA@DP*

To demonstrate the mechanism of action of GIPA@DP, RNA sequencing analysis of MV-4-11 cells after treatment with PBS, GIPA@P or GIPA@DP was performed. For the GIPA@DP group, CD38-upregulated MV-4-11 cells were used. As shown in Fig. 2A, GIPA@P treatment induced 766 differentially expressed genes (227 up, 539 down) compared with PBS, and GIPA@DP treatment further differentially regulated 3595 genes (1796 up and 1799 down versus the GIPA@P group). A Venn diagram further revealed the relationships of genes among the three groups (Fig. 2B). Principal component analysis (PCA) revealed that GIPA@P treatment drastically regulated the gene expression profile, and treatment with GIPA@DP further substantially reprogrammed gene expression compared with GIPA@P or PBS treatment (Fig. 2C). Kyoto Encyclopedia of Genes and Genomes (KEGG) analysis was then performed to evaluate the pathway enrichment of differentially expressed genes. GIPA@P treatment inhibited the cell cycle, DNA replication and DNA damage repair pathways that favor tumor growth [42–44], and activated hematopoietic cell lineage, phagosome, p53 signaling and immune response-related pathways that are beneficial for suppressing AML progression (Fig. 2D). Moreover, compared with GIPA@P treatment, GIPA@DP treatment further activated endocytosis, apoptosis, p53 signaling, and immune response pathways as well as signaling pathways regulating the pluripotency of stem cells. Notably, the activation of the endocytosis pathway is consistent with our findings that CD38 upregulation promoted the uptake of daratumumab-directed polymersomes in AML cells.

Gene set enrichment analysis (GSEA) revealed that, compared with GIPA@P, GIPA@DP induced positive enrichment in endocytosis, signaling pathways regulating pluripotency of stem cells, p53 signaling pathways and apoptosis (Fig. 2E). Gene Ontology (GO) analysis further confirmed that GIPA@P downregulated genes associated with cell cycle phase transition, DNA replication and repair but upregulated genes involved in cell differentiation and endocytosis (**Fig. S16**). These effects were further enhanced by treatment with GIPA@DP. Consistent with these observations, GIPA@DP significantly regulated genes associated with endocytosis (CD38, PICALM, RAB5B, etc.), the cell cycle (CDK4, CDK6, MYC, etc.), differentiation (CEBPB, IL6ST, SMAD5), apoptosis (BCL-2, the caspase family, PTEN, etc.) and dephosphorylation (DUSP4, the PTP family) (Fig. 2F).

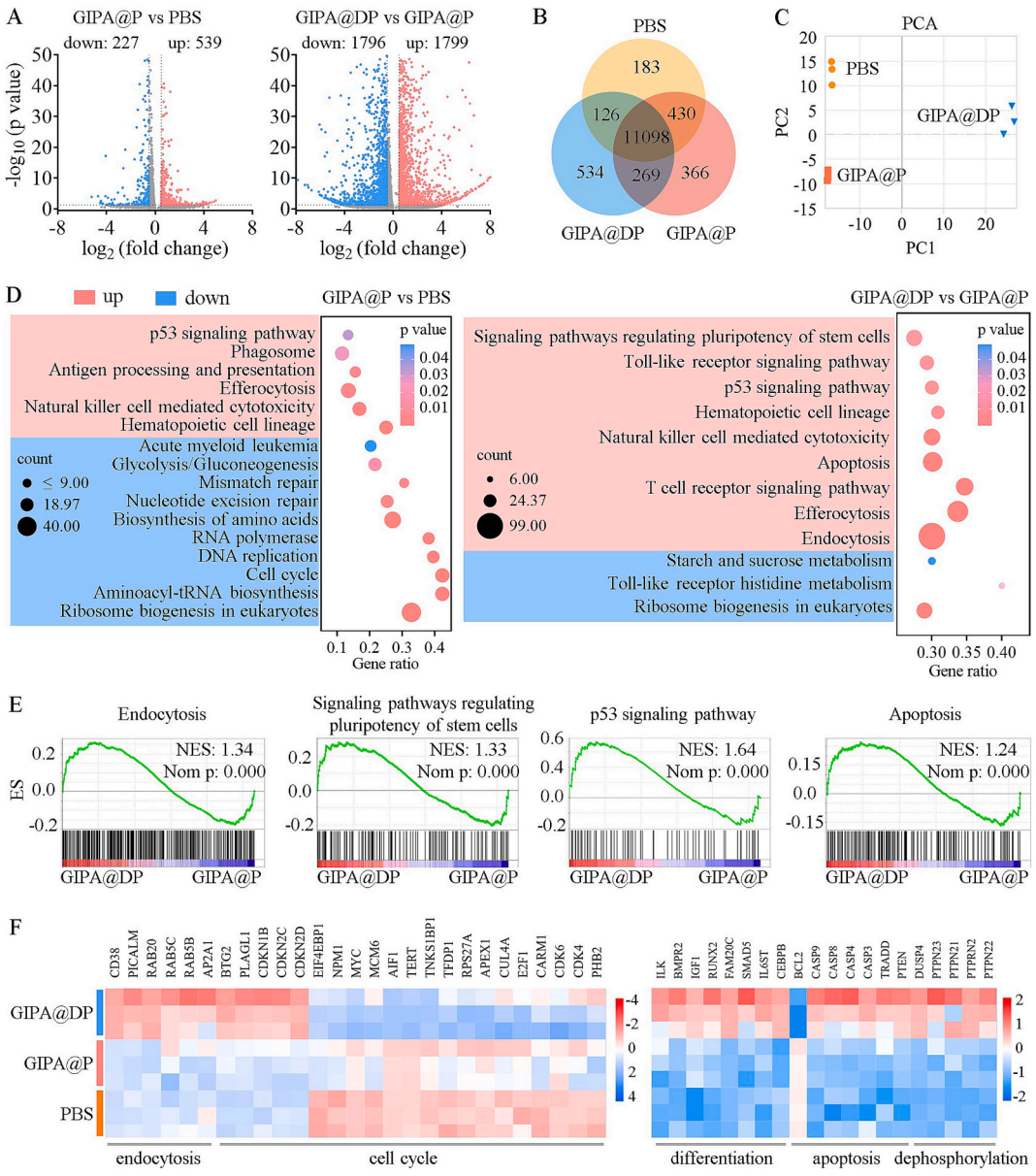

Fig. 2. Transcriptome analysis reveals the mechanisms of GIPA@DP treatment in MV-4-11 cells ($n = 3$). (A) Volcano plots showing differentially expressed genes in GIPA@P vs PBS and GIPA@DP vs GIPA@P. Genes with p values < 0.05 and absolute log2-fold changes > 0.5 were identified as differentially expressed genes. (B) Venn diagram showing the interactions between different groups. (C) PCA diagram of different groups. (D) KEGG pathway enrichment in the GIPA@P vs PBS and GIPA@DP vs GIPA@P comparisons. (E) GSEA plots illustrating the regulation of endocytosis, signaling pathways regulating the pluripotency of stem cells, the p53 signaling pathway and apoptosis in GIPA@DP-treated cells compared with GIPA@P-treated cells. (F) Heatmaps of differentially expressed genes related to endocytosis, the cell cycle, differentiation, apoptosis and dephosphorylation. CD38-upregulated MV-4-11 cells were used for the GIPA@DP group.

3.4. GIPA@DP enables ratiometric drug delivery and selective AML targeting in vivo

The in vivo pharmacokinetics and plasma drug ratios of different GIPA formulations were evaluated in healthy BALB/c mice via tail vein injection of free GIPA, GIPA@P or GIPA@DP. GIPA@P and GIPA@DP presented similar pharmacokinetic profiles, which significantly prolonged and unified the circulation of GI and PA (Fig. 3A **and Table S5**). Consequently, GIPA@P and GIPA@DP maintained a relatively stable plasma GI-to-PA ratio of approximately 1/1 within 48 h, in contrast to free GIPA with a drug ratio that deviated to 25/1 after only 4 h (Fig. 3B). The biodistribution of drugs was then studied in orthotopic MV-4-11-bearing mice via GIPA and Did-coloaded polymersomes (GIPA/Did@DP and GIPA/Did@P). For the GIPA/Did@DP group, a CD38-upregulated model was established by injecting ATRA for two consecutive days prior to each injection with daratumumab-polymersome formulations (Fig. 3C). The same procedure was applied in the subsequent in vivo studies. In vivo and ex vivo imaging revealed that treatment with GIPA/Did@DP led to significantly higher Did enrichment at primary leukemia infiltration sites, including the hindlimbs, forelimbs, liver and lung, compared with that of GIPA/Did@P (Fig. 3D,E **and S17**). Consistently, drug quantification via HPLC further confirmed the increased accumulation of GI in various tissues of the mice treated with GIPA/Did@DP (Fig. 3F). Moreover, both GIPA/Did@DP and GIPA/Did@P maintained relatively constant GI-to-PA ratios (0.78–1.37) in different tissues (Fig. 3G), supporting ratiometric drug codelivery by the polymersomes. Then, Cy5-labeled polymersomes (DP-Cy5 and P-Cy5) were further used to assess the AML selectivity of DP-Cy5 in CD38-upregulated orthotopic MV-4-11 AML-bearing mice. Notably, DP-Cy5 selectively bound to AML cells in different tissues,

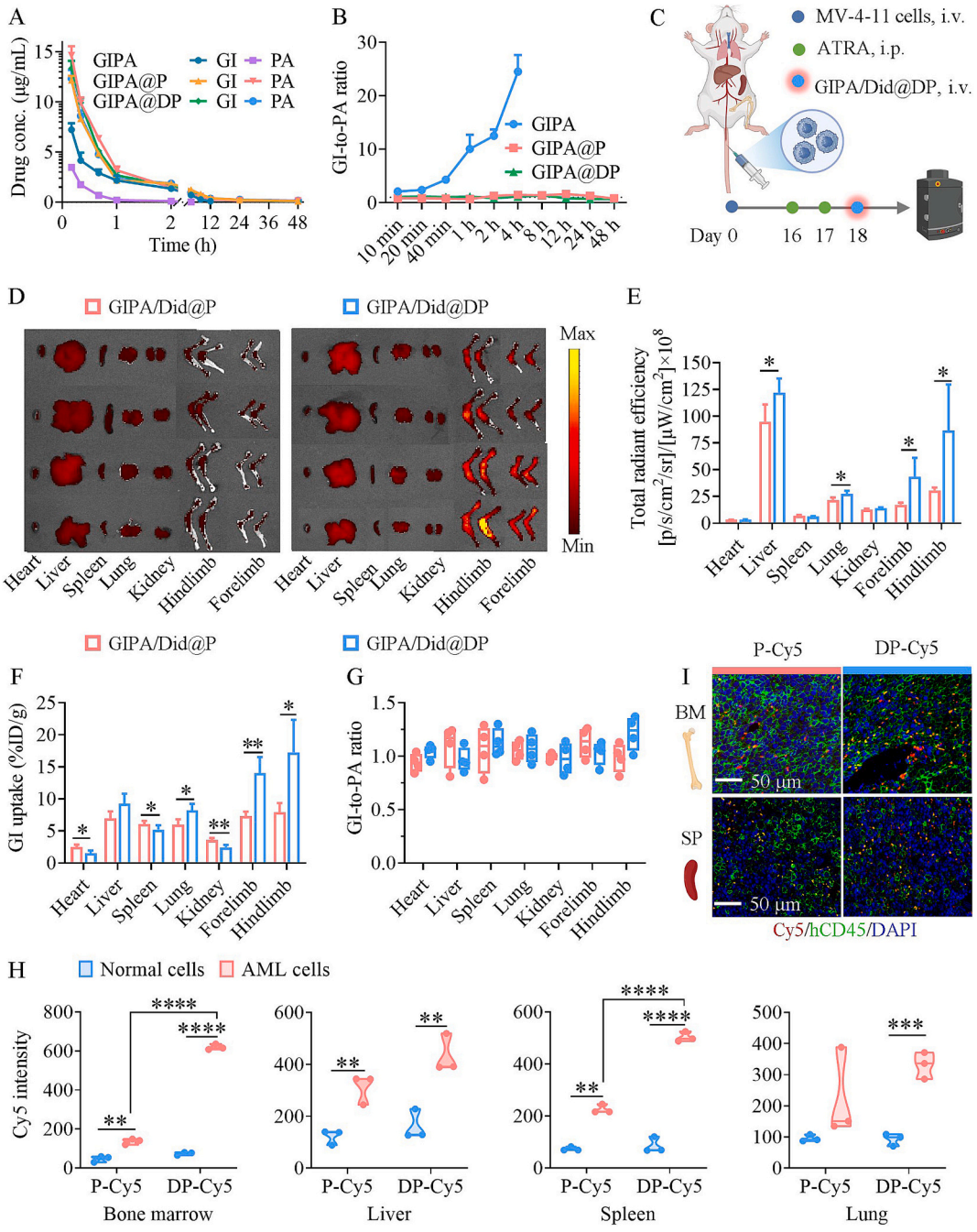

Fig. 3. In vivo ratiometric drug codelivery and selective AML targeting of GIPA@DP. (A) In vivo pharmacokinetics of free GIPA, GIPA@P and GIPA@DP in BALB/c mice. (B) Plasma GI-to-PA ratios at different time points. (C) Schematic of the protocol for the biodistribution study of GIPA/Did@DP in a CD38-upregulated orthotopic MV-4-11 AML model. Nontargeted GIPA/Did@P in the same model without CD38 upregulation served as a control. (D) Ex vivo fluorescence images and (E) quantitative fluorescence analysis of major organs and limbs isolated from mice at 8 h after injection with GIPA/Did@P or GIPA/Did@DP ($n = 4$). (F) The accumulation of GI in different tissues and (G) the corresponding GI-to-PA ratios at 8 h post-injection. (H) Selective AML binding of DP-Cy5 in different tissues ($n = 3$). (I) Immunofluorescence images showing the colocalization of DP-Cy5 with FITC-hCD45-stained AML cells (green) in the bone marrow (BM) and spleen (SP). Scale bars are 50 μm.

resulting in 2.7–8.3-fold stronger Cy5 fluorescence than that in normal cells (Fig. 3H). Compared with nontargeted P-Cy5, DP-Cy5 exhibited significantly enhanced binding to AML cells while maintaining a similar binding affinity to normal cells. Immunofluorescence images of the bone marrow and spleen further revealed strong colocalization of DP-Cy5 with FITC anti-human CD45 antibody (hCD45)-stained AML cells (Fig. 3I).

3.5. GIPA@DP effectively inhibits leukemia progression in vivo

The anti-AML efficacy of GIPA@DP was first investigated in orthotopic MV-4-11 AML-bearing mice, with GI@P, PA@P, free GIPA, GIPA@P and a mixture of single drug-loaded daratumumab polymersomes (GI@DP+PA@DP) serving as controls. Different GI and/or PA formulations were intravenously injected every 2 days at GI and PA dosages of 8 mg/kg for 6 times (Fig. 4A). For the GIPA@DP and GI@DP+PA@DP groups, the CD38-upregulated MV-4-11 model was

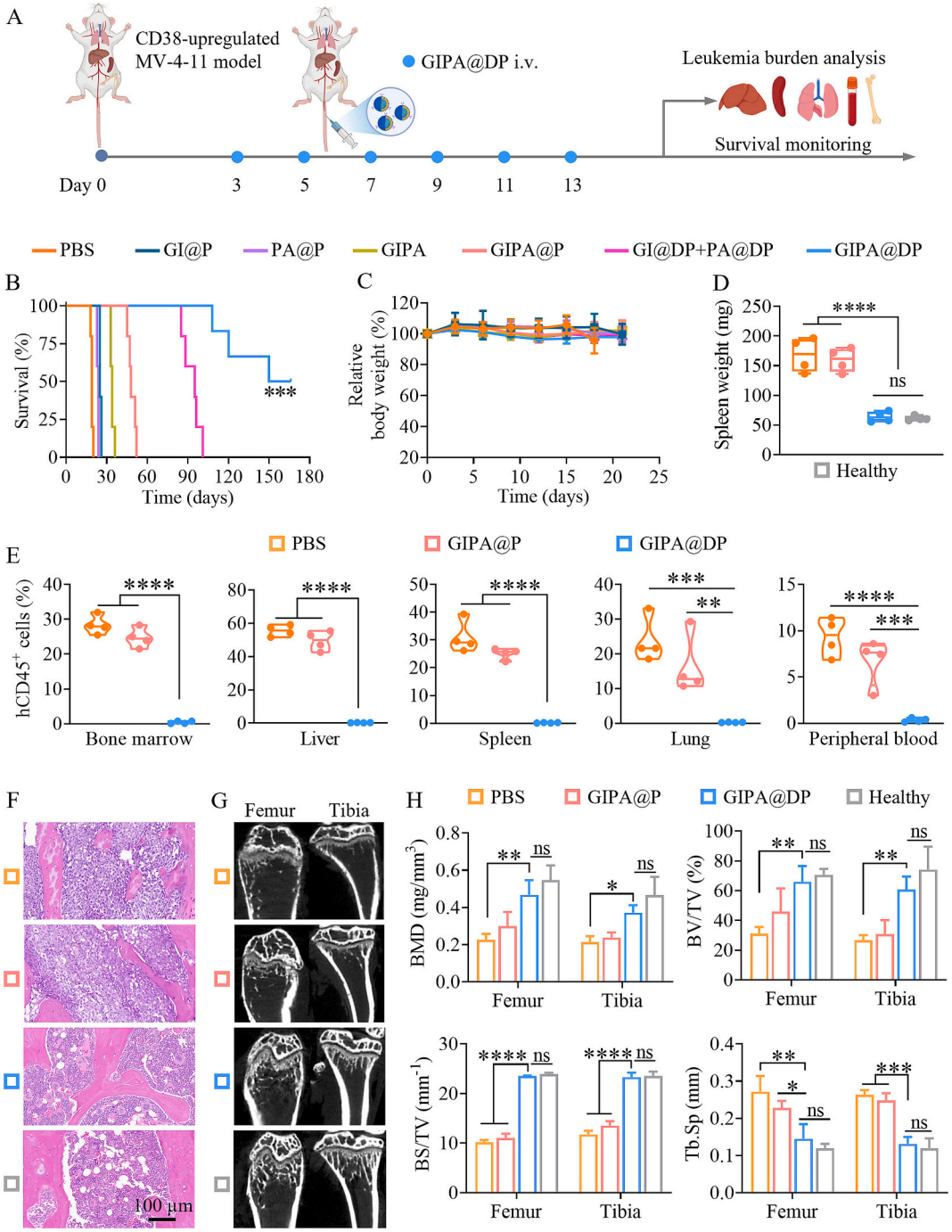

Fig. 4. Anti-AML efficacy of GIPA@DP in CD38-upregulated orthotopic MV-4-11 mice. (A) Treatment and monitoring scheme. (B) Survival curves of the mice after different treatments ($n = 5$). GIPA@DP vs all other controls, $^{***}p < 0.001$. (C) Body weight changes of the mice after different treatments (n = 5). (D) Weights of spleens isolated from mice in different groups, with healthy mice serving as a control ($n = 3$). (E) Percentages of AML cells in the bone marrow, liver, spleen, lung and peripheral blood (n = 3). (F) Representative H&E-stained images of bone marrow harvested from mice in different groups (scale bar: 100 μm). (G) Representative micro-CT images of femurs and tibias extracted from mice in different groups. (H) Quantitative analysis of the femur- and tibia-related parameters (n = 3).

employed. In the PBS-treated group, MV-4-11 cells rapidly proliferated and substantially infiltrated the bone marrow, liver, spleen, lung and blood on day 18, leading to rapid mortality, with a median survival time (MST) of 19 days (Fig. 4B**, S18**). GIPA@P treatment significantly prolonged the survival of the mice (MST: 48 days), which was in sharp contrast to the findings that GI@P and PA@P single drug polymersomes had limited survival benefits (MST: 24 and 25 days) and free GIPA (MST: 34 days), suggesting that GIPA@P has synergistic effects with ratiometric drug delivery. Notably, GIPA@DP treatment further remarkably extended the survival of the mice, with 50 % of the mice surviving for at least 165 days (Fig. 4B). This outcome significantly outperformed that of the GI@DP+PA@DP treatment (MST: 95 days), supporting the importance of *co*-formulating two drugs in one polymersome. Moreover, there were no significant body weight changes in the mice that received different treatments (Fig. 4C). The absence of splenomegaly, a typical feature in AML patients [45,46], in GIPA@DP-treated mice provided additional evidence (Fig. 4D). Furthermore, GIPA@DP treatment almost completely depleted the leukemia burden in various tissues and was superior to GIPA@P treatment (Fig. 4E**, S18**). Consistently, H&E staining revealed obvious leukemia infiltration in the bone marrow, spleen

and lung of the mice in the PBS and GIPA@P groups; however, this infiltration was significantly alleviated in the GIPA@DP-treated mice with similar histological appearance of all organs to that of the healthy mice (Fig. 4F, **S19**).

Leukemia progression in the bone marrow often results in osteolytic destruction [47]. Therefore, micro-CT imaging was performed to observe and analyze the internal structure of the hindlimbs of mice following different treatments. As visualized in Fig. 4G, GIPA@DP treatment completely prevented osteolysis, and the bone structure of the mice was similar to that of the healthy mice, which contrasted sharply with that of the mice in the PBS and GIPA@P groups, with obvious bone destruction in the femur and tibia. The quantitative data further confirmed that the bone microstructure parameters of the femurs and tibias of the GIPA@DP-treated mice, including the bone mineral density (BMD), bone volume fraction (BV/TV), bone surface area/bone volume (BS/TV), trabecular separation (Tb.Sp), and trabecular number and thickness, were comparable to those of the healthy mice (Fig. 4H, **S20A**). Increased osteoclasts as a result of leukemia infiltration in the bone marrow are one of the primary causes of osteolysis [48]. We then stained the hindlimbs of the mice with TRAP, a characteristic marker of osteoclasts [49], to detect osteoclasts. The results revealed that the number of osteoclasts in GIPA@DP-treated mice was obviously lower

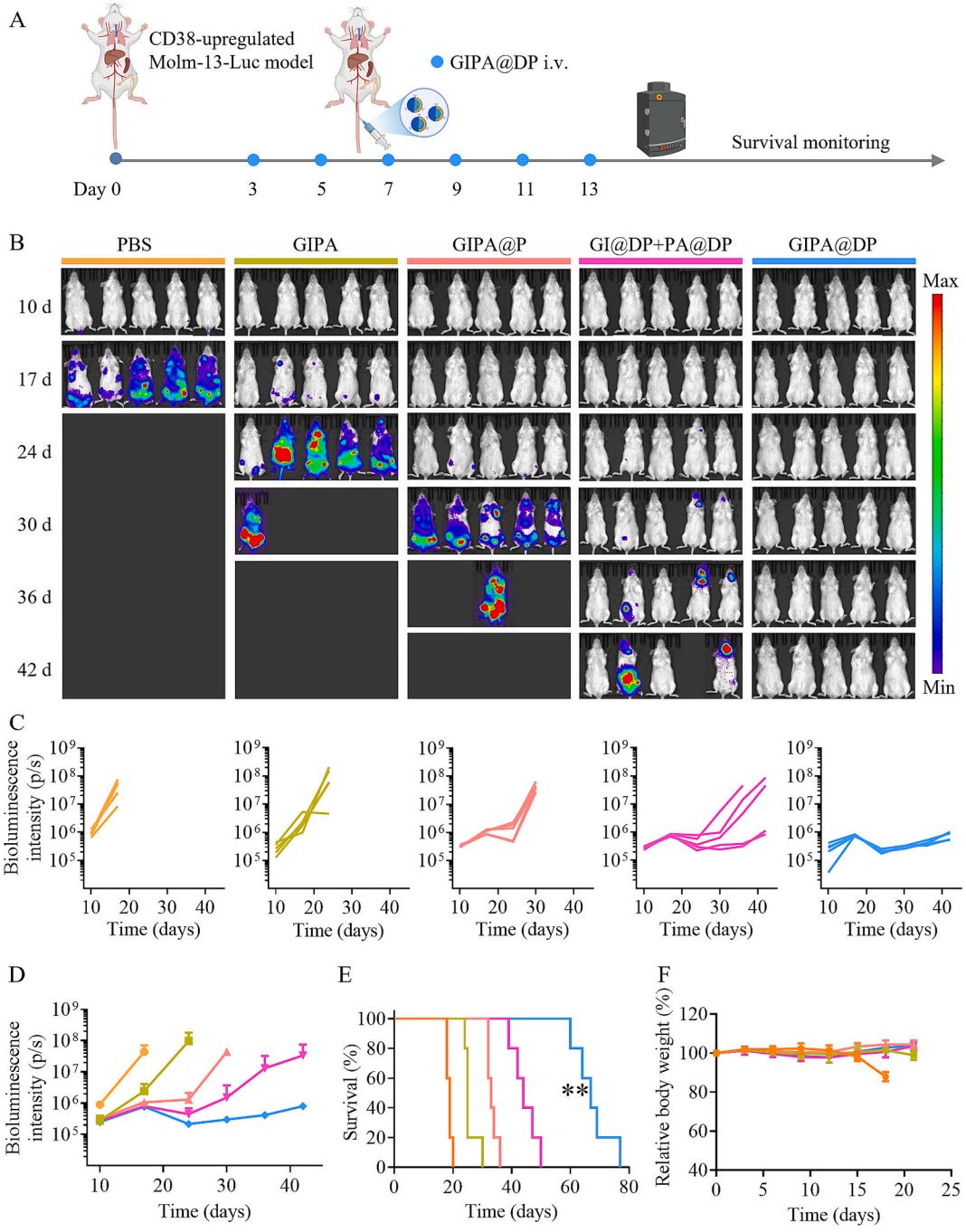

Fig. 5. Anti-AML activity of GIPA@DP in CD38-upregulated orthotopic Molm-13-Luc mice. (A) Treatment and monitoring schedule. (B) Bioluminescence images of the mice treated with PBS, GIPA, GIPA@P, GI@DP+PA@DP or GIPA@DP. (C) Quantitative analysis of bioluminescence signals from each individual mouse and (D) the average intensity in different groups. (E) Survival curves (GIPA@DP vs all control groups, $^{**}p < 0.01$) and (F) body weight changes of the mice after different treatments ($n = 5$).

than that in control mice but was comparable to that in healthy mice (**Fig. S20B**).

To further validate the anti-AML efficacy of GIPA@DP, an orthotopic Molm-13-Luc AML mouse model was established and treated under the same schedule and drug dosage as the MV-4-11 model (Fig. 5A). The treatments included PBS, GIPA, GIPA@P, GI@DP+PA@DP and GIPA@DP, and the last two groups were studied in a CD38-upregulated model. Bioluminescence images revealed that Molm-13-Luc AML cells proliferated exponentially in the mice, leading to a short MST of 19 days (Fig. 5B-E). Treatment with free GIPA slightly retarded leukemia growth by approximately 1 week. In contrast, GIPA@DP significantly inhibited leukemia proliferation, with no detectable bioluminescence signals for at least 42 days, outperforming GIPA@P and GI@DP+PA@DP (Fig. 5B-D). As a result, GIPA@DP effectively prolonged the survival of mice with an MST of 67 days, which was markedly longer in comparison to that of the PBS, GIPA (25 days), GIPA@P (33 days) and GI@DP+PA@DP (44 days) groups (Fig. 5E). Importantly, all the treatments were well tolerated by the mice, with no significant decrease in body weight observed (Fig. 5F).

4. Conclusions

In this study, we have demonstrated that daratumumab-polymersome mediated ratiometric codelivery of GI and PA dual inhibitors (GIPA@DP) enables high-efficacy coinhibition of FLT3 and CDK4/6 and potentiates targeted therapy of AML. GIPA@DP selectively targeted AML cells and enhanced drug delivery to CD38-upregulated AML cells, resulting in potent synergistic effects on the induction of cell apoptosis and differentiation. Moreover, GIPA@DP was effectively enriched in the bone marrow and other leukemia-infiltrated organs of CD38-upregulated AML-bearing mice with synergistic drug ratios and selectively targeted AML cells, thus significantly inhibiting leukemia progression in different AML models. Strikingly, GIPA@DP treatment markedly improved survival, with 50 % of the mice achieving remission in the CD38-upregulated MV-4-11 AML model, significantly outperforming nontargeted GIPA@P and a mixture of two single drug-loaded targeting polymersomes (GI@DP+PA@DP). This antibody-targeted ratiometric codelivery of dual inhibitors may provide a new and promising targeted therapy for AML.

CRediT authorship contribution statement

Zhenzhen Zhai: Writing – original draft, Methodology, Investigation, Formal analysis, Data curation, Conceptualization. **Chenming Li:** Methodology, Investigation, Formal analysis. **Lin Chen:** Methodology, Investigation, Data curation. **Yan Zhao:** Methodology, Investigation. **Xueling Tang:** Methodology, Investigation. **Li Cao:** Resources, Methodology. **Huanli Sun:** Writing – review & editing, Supervision, Project administration, Methodology, Funding acquisition, Conceptualization. **Zhiyuan Zhong:** Writing – review & editing, Supervision, Resources, Project administration, Funding acquisition, Conceptualization.

Declaration of competing interest

The authors declare no competing financial interest.

Acknowledgements

This work was supported by the National Key Research and Development Program of China (2021YFB3800900), and the National Natural Science Foundation of China (52273251 and 52473264). The schemes in the figures were created with BioRender.com.

Appendix A. Supplementary data

Supplementary data to this article can be found online at https://doi.org/10.1016/j.jconrel.2025.113934.

Data availability

Data will be made available on request.

References

[1] R. Santos, O. Ursu, A. Gaulton, A.P. Bento, R.S. Donadi, C.G. Bologa, A. Karlsson, B. Al-Lazikani, A. Hersey, T.I. Oprea, J.P. Overington, A comprehensive map of molecular drug targets, Nat. Rev. Drug Discov. 16 (2017) 19–34.
[2] P.L. Bedard, D.M. Hyman, M.S. Davids, L.L. Siu, Small molecules, big impact: 20 years of targeted therapy in oncology, Lancet 395 (2020) 1078–1088.
[3] Y. Zhou, L. Tao, J. Qiu, J. Xu, X. Yang, Y. Zhang, X. Tian, X. Guan, X. Cen, Y. Zhao, Tumor biomarkers for diagnosis, prognosis and targeted therapy, Signal Transduct. Target. Ther. 9 (2024) 132.
[4] H. Jin, L. Wang, R. Bernards, Rational combinations of targeted cancer therapies: background, advances and challenges, Nat. Rev. Drug Discov. 22 (2023) 213–234.
[5] C.D. DiNardo, H.P. Erba, S.D. Freeman, A.H. Wei, Acute myeloid leukaemia, Lancet 401 (2023) 2073–2086.
[6] X. Xie, Y. Hu, T. Ye, Y. Chen, L. Zhou, F. Li, X. Xi, S. Wang, Y. He, X. Gao, W. Wei, G. Ma, Y. Li, Therapeutic vaccination against leukaemia via the sustained release of co-encapsulated anti-PD-1 and a leukaemia-associated antigen, Nat. Biomed. Eng. 5 (2021) 414–428.
[7] J. Schaefer, S. Cassidy, R.M. Webster, The acute myeloid leukaemia market, Nat. Rev. Drug Discov. 19 (2020) 233–234.
[8] H.M. Kantarjian, C.D. DiNardo, T.M. Kadia, N.G. Daver, J.K. Altman, E.M. Stein, E. Jabbour, C.A. Schiffer, A. Lang, F. Ravandi, Acute myeloid leukemia management and research in 2025, CA Cancer, J. Clin. Densitom. 75 (2025) 46–67.
[9] R.S. Bhansali, K.W. Pratz, C. Lai, Recent advances in targeted therapies in acute myeloid leukemia, J. Hematol. Oncol. 16 (2023) 29.
[10] A.I. Antar, Z.K. Otrock, E. Jabbour, M. Mohty, A. Bazarbachi, FLT3 inhibitors in acute myeloid leukemia: ten frequently asked questions, Leukemia 34 (2020) 682–696.
[11] H. Döhner, A.H. Wei, B. Löwenberg, Towards precision medicine for AML, Nat. Rev. Clin. Oncol. 18 (2021) 577–590.
[12] S. Boumahdi, F.J. de Sauvage, The great escape: tumour cell plasticity in resistance to targeted therapy, Nat. Rev. Drug Discov. 19 (2020) 39–56.
[13] M.T. Gebru, H.-G. Wang, Therapeutic targeting of FLT3 and associated drug resistance in acute myeloid leukemia, J. Hematol. Oncol. 13 (2020) 155.
[14] Z. Wang, J. Cai, J. Cheng, W. Yang, Y. Zhu, H. Li, T. Lu, Y. Chen, S. Lu, FLT3 inhibitors in acute myeloid leukemia: challenges and recent developments in overcoming resistance, J. Med. Chem. 64 (2021) 2878–2900.
[15] D. Capelli, D. Menotti, A. Fiorentini, F. Saraceni, A. Olivieri, Overcoming resistance: FLT3 inhibitors past, present, future and the challenge of cure, Cancers 14 (2022) 4315.
[16] J. Yang, R. Friedman, Combination strategies to overcome drug resistance in FLT+ acute myeloid leukaemia, Cancer Cell Int. 23 (2023) 161.
[17] S. Goel, J.S. Bergholz, J.J. Zhao, Targeting CDK4 and CDK6 in cancer, Nat. Rev. Cancer 22 (2022) 356–372.
[18] V.Y. Ling, J. Straube, W. Godfrey, R. Haldar, Y. Janardhanan, L. Cooper, C. Bruedigam, E. Cooper, P. Tavakoli Shirazi, S. Jacquelin, S.-K. Tey, J. Baell, F. Huang, J. Jin, Y. Zhao, L. Bullinger, M.J. Bywater, S.W. Lane, Targeting cell cycle and apoptosis to overcome chemotherapy resistance in acute myeloid leukemia, Leukemia 37 (2023) 143–153.
[19] L. Zhong, Y. Li, L. Xiong, W. Wang, M. Wu, T. Yuan, W. Yang, C. Tian, Z. Miao, T. Wang, S. Yang, Small molecules in targeted cancer therapy: advances, challenges, and future perspectives, Signal Transduct. Target. Ther. 6 (2021) 201.
[20] Y. Zhang, C.P. Hsu, J.F. Lu, M. Kuchimanchi, Y.N. Sun, J. Ma, G. Xu, Y. Zhang, Y. Xu, M. Weidner, J. Huard, D.Z. D'Argenio, FLT3 and CDK4/6 inhibitors: signaling mechanisms and tumor burden in subcutaneous and orthotopic mouse models of acute myeloid leukemia, J. Pharmacokinet. Pharmacodyn. 41 (2014) 675–691.
[21] I.Z. Uras, G.J. Walter, R. Scheicher, F. Bellutti, M. Prchal-Murphy, A.S. Tigan, P. Valent, F.H. Heidel, S. Kubicek, C. Scholl, S. Fröhling, V. Sexl, Palbociclib treatment of FLT3-ITD+ AML cells uncovers a kinase-dependent transcriptional regulation of FLT3 and PIM1 by CDK6, Blood 127 (2016) 2890–2902.
[22] R.X. Zhang, H.L. Wong, H.Y. Xue, J.Y. Eoh, X.Y. Wu, Nanomedicine of synergistic drug combinations for cancer therapy – strategies and perspectives, J. Control. Release 240 (2016) 489–503.
[23] A. Detappe, H.V.T. Nguyen, Y. Jiang, M.P. Agius, W. Wang, C. Mathieu, N.K. Su, S. L. Kristufek, D.J. Lundberg, S. Bhagchandani, I.M. Ghobrial, P.P. Ghoroghchian, J. A. Johnson, Molecular bottlebrush prodrugs as mono- and triplex combination therapies for multiple myeloma, Nat. Nanotechnol. 18 (2023) 184–192.
[24] Y. Sun, H. Hu, X. Jing, Q. Meng, B. Yu, H. Cong, Y. Shen, Co-delivery of chemotherapeutic drugs and cell cycle regulatory agents using nanocarriers for cancer therapy, Sci. China Mater. 64 (2021) 1827–1848.
[25] L. Sun, H. Liu, Y. Ye, Y. Lei, R. Islam, S. Tan, R. Tong, Y.-B. Miao, L. Cai, Smart nanoparticles for cancer therapy, Signal Transduct. Target. Ther. 8 (2023) 418.
[26] P. Tardi, S. Johnstone, N. Harasyrn, S.W. Xie, T. Harasyrn, N. Zisman, P. Harvie, D. Bermudes, L. Mayer, In vivo maintenance of synergistic cytarabine: Daunorubicin ratios greatly enhances therapeutic efficacy, Leuk. Res. 33 (2009) 129–139.

[27] J.E. Lancet, J.E. Cortes, D.E. Hogge, M.S. Tallman, T.J. Kovacsovics, L.E. Damon, R. Komrokji, S.R. Solomon, J.E. Kolitz, M. Cooper, A.M. Yeager, A.C. Louie, E. J. Feldman, Phase 2 trial of CPX-351, a fixed 5:1 molar ratio of cytarabine/daunorubicin, vs cytarabine/daunorubicin in older adults with untreated AML, Blood 123 (2014) 3239–3246.
[28] J.E. Lancet, G.L. Uy, J.E. Cortes, L.F. Newell, T.L. Lin, E.K. Ritchie, R.K. Stuart, S. A. Strickland, D. Hogge, S.R. Solomon, R.M. Stone, D.L. Bixby, J.E. Kolitz, G. J. Schiller, M.J. Wieduwilt, D.H. Ryan, A. Hoering, K. Banerjee, M. Chiarella, A. C. Louie, B.C. Medeiros, CPX-351 (cytarabine and daunorubicin) liposome for injection versus conventional cytarabine plus daunorubicin in older patients with newly diagnosed secondary acute myeloid leukemia, J. Clin. Oncol. 36 (2018) 2684–2692.
[29] W. Gu, F. Meng, R. Haag, Z. Zhong, Actively targeted nanomedicines for precision cancer therapy: concept, construction, challenges and clinical translation, J. Control. Release 329 (2021) 676–695.
[30] Y. Xia, J. An, J. Li, W. Gu, Y. Zhang, S. Zhao, C. Zhao, Y. Xu, B. Li, Z. Zhong, F. Meng, Transferrin-guided intelligent nanovesicles augment the targetability and potency of clinical PLK1 inhibitor to acute myeloid leukemia, Bioact. Mater. 21 (2023) 499–510.
[31] J. Du, S. Yue, C. Li, J. Li, S. Zhao, Y. Dong, Y. Zhang, R. Cheng, H. Sun, Z. Zhong, Exogenous CD38 upregulation enables high-efficacy dually cascade targeted molecular therapy of leukemia, Nano Today 50 (2023) 101872.
[32] S.J. Yue, J.N. An, Y.F. Zhang, J.Y. Li, C.Z. Zhao, J.Y. Liu, L.L. Liang, H.L. Sun, Y. Xu, Z.Y. Zhong, Exogenous antigen upregulation empowers antibody targeted nanochemotherapy of leukemia, Adv. Mater. 35 (2023) 2209984.
[33] K. McKeage, Daratumumab: First global approval, Drugs 76 (2016) 275–281.
[34] J.E. Maakaron, C. Seichter, R. Wangen, A. Hoeschen, D. Kolaseri Krishnadas, K. Kent, R. Shanley, D. O'Leary, N.H. El Jurdi, S.G. Holtan, B. Betts, M. Juckett, J. S. Miller, Phase I study of FT538 + daratumumab for treatment of r/r AML, Blood 142 (2023) 4842.
[35] N. Yu, Y. Zhang, J. Li, W. Gu, S. Yue, B. Li, F. Meng, H. Sun, R. Haag, J. Yuan, Z. Zhong, Daratumumab immunopolymersome-enabled safe and CD38-targeted chemotherapy and depletion of multiple myeloma, Adv. Mater. 33 (2021) 2007787.
[36] M.M. Dzama, M. Steiner, J. Rausch, D. Sasca, J. Schönfeld, K. Kunz, M.C. Taubert, G.M. McGeehan, C.-W. Chen, A. Mupo, P. Hähnel, M. Theobald, T. Kindler, R. P. Koche, G.S. Vassiliou, S.A. Armstrong, M.W.M. Kühn, Synergistic targeting of FLT3 mutations in AML via combined menin-MLL and FLT3 inhibition, Blood 136 (2020) 2442–2456.
[37] X. Xie, W. Zhang, X. Zhou, Z. Ye, H. Wang, Y. Qiu, Y. Pan, Y. Hu, L. Li, Z. Chen, W. Yang, Y. Lu, S. Zou, Y. Li, X. Bai, Abemaciclib drives the therapeutic differentiation of acute myeloid leukaemia stem cells, Br. J. Haematol. 201 (2023) 940–953.
[38] K. Reiter, H. Polzer, C. Krupka, A. Maiser, B. Vick, M. Rothenberg-Thurley, K. H. Metzeler, D. Dörfel, H.R. Salih, G. Jung, E. Nössner, I. Jeremias, W. Hiddemann, H. Leonhardt, K. Spiekermann, M. Subklewe, P.A. Greif, Tyrosine kinase inhibition increases the cell surface localization of FLT3-itd and enhances FLT3-directed immunotherapy of acute myeloid leukemia, Leukemia 32 (2018) 313–322.
[39] K.-X. Li, H.-Y. Wu, W.-Y. Pan, M.-Q. Guo, D.-Z. Qiu, Y.-J. He, Y.-H. Li, D.-H. Yang, Y.-X. Huang, A novel approach for relapsed/refractory FLT3mut+ acute myeloid leukaemia: synergistic effect of the combination of bispecific FLT3scFv/NKG2D-CAR T cells and gilteritinib, Mol. Cancer 21 (2022) 66.
[40] M.C. Nawijn, A. Alendar, A. Berns, For better or for worse: the role of pim oncogenes in tumorigenesis, Nat. Rev. Cancer 11 (2011) 23–34.
[41] P.J. Sung, M. Selvam, S.S. Riedel, H.M. Xie, K. Bryant, B. Manning, G.B. Wertheim, K. Kulej, L. Pham, R.L. Bowman, J. Peresie, M.J. Nemeth, R.L. Levine, B.A. Garcia, S.E. Meyer, S. Sidoli, K.M. Bernt, M. Carroll, FLT3 tyrosine kinase inhibition modulates PRC2 and promotes differentiation in acute myeloid leukemia, Leukemia 38 (2024) 291–301.
[42] E.M. Michalak, M.L. Burr, A.J. Bannister, M.A. Dawson, The roles of DNA, RNA and histone methylation in ageing and cancer, Nat. Rev. Mol. Cell Biol. 20 (2019) 573–589.
[43] H.K. Matthews, C. Bertoli, R.A.M. de Bruin, Cell cycle control in cancer, Nat. Rev. Mol. Cell Biol. 23 (2022) 74–88.
[44] F.J. Groelly, M. Fawkes, R.A. Dagg, A.N. Blackford, M. Tarsounas, Targeting DNA damage response pathways in cancer, Nat. Rev. Cancer 23 (2023) 78–94.
[45] L. Kumar, H. Menon, A. Sharma, J. Wadhwa, R. Kumar, V. Kochupillai, Acute myeloid leukemia (AML): a study of 516 patients, J. Clin. Oncol. 22 (2004) 6711.
[46] G.H.D.M. Oliveira, L.S.D.S. Júnior, A.E.M.O.E. Silva, J.P.A. Lima, V.L. Soares, R. V. Freitas, T.M. Oliveira, D.G.K.C. Silva, V.S. Sales, H.D.D.O. Paiva, R.S. Araujo, A. S. Paiva, G.B. Cavalcanti, A.S.J. Silva, Clinical utility of flow cytometry immunophenotyping in acute myeloid leukemia, Blood 134 (2019) 5191.
[47] O.J. Tamplin, Chewing through roots: how leukemia invades and disrupts the bone marrow microenvironment, Cell Stem Cell 22 (2018) 5–7.
[48] E. Dondossola, S. Alexander, B.M. Holzapfel, S. Filippini, M.W. Starbuck, R. M. Hoffman, N. Navone, E.M. De-Juan-Pardo, C.J. Logothetis, D.W. Hutmacher, P. Friedl, Intravital microscopy of osteolytic progression and therapy response of cancer lesions in the bone, Sci. Transl. Med. 10 (2018) eaao5726.
[49] Y. Yahara, T. Barrientos, Y.J. Tang, V. Puviindran, P. Nadesan, H. Zhang, J. R. Gibson, S.G. Gregory, Y. Diao, Y. Xiang, Y.J. Qadri, T. Souma, M.L. Shinohara, B. A. Alman, Erythromyeloid progenitors give rise to a population of osteoclasts that contribute to bone homeostasis and repair, Nat. Cell Biol. 22 (2020) 49–59.